

Experimental Modeling of Temperature Rise of Mass Concrete by FDM Method

D S Guo, E Y Chen*, G L Low and J L Yang

SsangYong Cement (Singapore) Limited
17 Pioneer Crescent, Singapore 628552

(*To whom all correspondences shall be addressed)

Abstract

Experimental tests were carried out to investigate the temperature rise characteristics of high slag blastfurnace cement concrete under adiabatic conditions. Typical ground granulated blastfurnace slag (GGBS) with Blaine fineness of 500 m²/kg was used and the slag replacement ratio in cement was up to 90%. An estimation method was successfully adopted and modified based on lab test results to simulate the temperature development history of the concrete under adiabatic conditions. For the evaluation of temperature rise and distribution in mass concrete blocks, a simulated heat generation of concrete was obtained and incorporated with 2-D finite-difference thermal transfer numerical analysis. Effects of various factors, including cement content, GGBS replacing ratio of cement, insulation materials, placing temperature of concrete, etc., on the temperature rise and distribution in a mass concrete mockup block were discussed.

Test results found that the concrete with more than 50% GGBS replacement in cement exhibited a significant decrease in the peak value of the temperature rise and maximum temperature rise rate. The results of the numerical simulation showed that the temperature development and distribution profile, which is directly contributed from the heat of hydration of cement with time, is significantly affected by the selection of insulation, placing temperature and construction procedures.

Keywords: high slag blastfurnace cement, mass concrete, temperature rise, FDM method

1. Introduction

Temperature rise effects on mass concrete construction has been widely noticed [1, 2, 3, 4]. In general, the major concerns related to the temperature rise in mass concrete structure practice are concrete degradation and concrete cracking at early age. The degree of degradation of concrete in compressive strength, splitting tensile strength and Young's modulus of elasticity is significantly affected by the mass concrete curing temperature [5]. Basically, the higher and the longer the curing temperature, the lower the values of the resulted compressive strength, splitting strength and Young's modulus. The adverse effect of high temperature in concrete on the bond between the concrete and the embedded reinforcement was also reported [6]. The cracking of mass concrete at early age is attributed to the thermal tensile strain / stress, which is induced by the internal and external restrains under nonuniform temperature distribution across the concrete mass. To avoid concrete surface cracking caused by heat generated in the concrete, European Standard ENV 206: 1992 [7] suggests that the limit on the temperature difference between the center and the surface is 20°C and the average maximum temperature limit of concrete is 60°C. The limits imply that during the concrete heating and cooling period, the resulted thermal strain / stress, which is caused by

internal and external restraints under even higher temperature and higher temperature difference, may exceed the limit of the tensile strain / stress of the concrete.

Due to the reduced rate of hydration, the use of blastfurnace slag partially to replace OPC is one of the successful practices to considerably reduce the temperature rise in mass concrete [8]. An estimation of the heat hydration with blended cement is more complicated [4]. Moreover, a number of factors, such as cement type, type of the mineral additives, content of cementitious material, aggregate type, admixture, geometry and size of concrete mass, concrete placing temperature, insulation, and concrete construction sequence, etc., affect the temperature rise and temperature distribution profile in mass concrete. Concrete temperature rise test under adiabatic conditions is normally an approach in laboratory to evaluate the exothermic characteristics of the hydration of the concrete. Construction contractors often tend to use plain concrete trial block with an array of thermocouples to assess the characteristics of the temperature rise and the maximum temperature difference in the concrete. However, this approach could give misleading results if the relevant factors are neglected, such as concrete block size, insulation, thermal couple location and construction sequence.

The experimental program in the study was to investigate the temperature rise characteristics of high slag blastfurnace cement (HSPBFC) concrete under adiabatic conditions. The objective of the numerical program was to incorporate the heat generated by the concrete with FDM heat transfer analysis to simulate the temperature rise and distribution in mass concrete trial block. The temperature rise in a mass concrete trial block was presented. Results of the study and the developed analytical technique allow the better understanding of the temperature rise and distribution in the mass concrete trial block and actual mass concrete structures.

2. Raw materials and control concrete mix design

The concrete adiabatic temperature rise monitoring system and typical SsangYong commercial cements OPC and HSPBFC (P4246 containing 65% GGBS) have been reported elsewhere [8]. The physical properties and chemical compositions of the typical OPC, HSPBFC (P4246S) containing 70 ~ 75% GGBS used in the study are listed in Table 1 and Table 2. Table 3 presents the control design mix C40 for all the concrete tests. The measured placing temperature of the mixes was from 30°C to 32°C.

Table 1: OPC and HSPBFC (P4246S)

	Standard	Typical properties				
		Blaine fineness (m ² /kg)	Specific gravity	Initial setting time (min.)	2d strength (MPa)	28d strength (MPa)
OPC	BS 12 42.5R SS 26 42.5R	335	3.15	125	28	53
HSPBFC (P4246S)	BS 4246 SS 476	450	2.94	185	33 (3d)	51

Table2: Typical properties and chemical analysis of GGBS (BS 6699:1992)

Blaine fineness (m ² /Kg)	Specific gravity	Chemical composition (%)					
		SiO ₂	Al ₂ O ₃	Fe ₂ O ₃	CaO	MgO	SO ₃
500	2.85	32.5	13.3	0.8	39.0	4.4	2.0

Table 3: C40 concrete mix design

Cement (kg/m ³)	Water (l)	Sand (BS Zone I) (kg)	Crushed granite (20mm) (kg)	Admixture (Daracem 100) (l/100kg cement)	slump (mm)	28d strength (MPa)
405*	170	730	1020	0.9	100 ~ 150	≥ 50

* Comprising OPC and GGBS with percentage of 0, 20, 35, 50, 65, 70, 80, 90 respectively.

3. Experimental results and discussion

Effects of GGBS on the maximum temperature rise of concrete were clearly demonstrated from the experimental results. Figure 1 shows the typical curves of temperature rise and temperature rise rate for OPC and HSPBFC concrete under adiabatic conditions. The maximum rate of the temperature rise occurred in the early stage of cement hydration. For the concrete with different GGBS replacement ratio, Figure 2 shows the temperature rise at 72 hours after mix placing. The maximum temperature rise rate of concrete during the temperature development is also presented in Figure 2.

Test results in Figure 2 indicates that the GGBS content has significant effects on the adiabatic temperature rise and maximum temperature rise rate in concrete. With the GGBS content less than 50%, there is very marginal difference in the temperature rise. This effect also applies to the maximum temperature rise rate. When the GGBS content exceeds about 50%, the reduction of temperature rise and the maximum temperature rise rate become very significant. For concrete with commercial product P4246S (GGBS 70 ~ 75%), the temperature rise is about 20°C less than OPC for the same design mix, and the maximum temperature rise rate reduces about 72%.

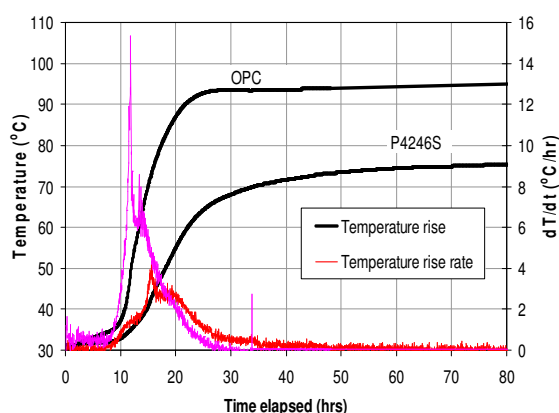


Figure 1: Typical temperature rise and temperature rise rate of OPC and P4246S concrete under adiabatic condition

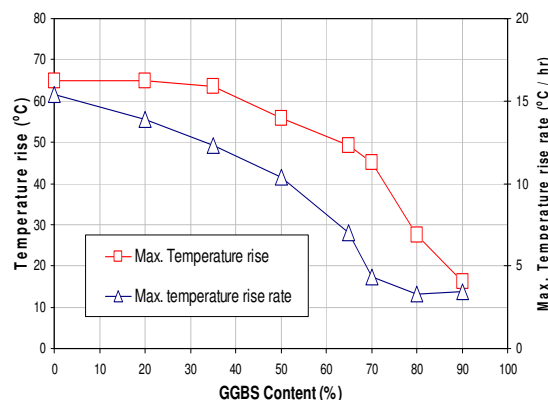


Figure 2: The temperature rise and maximum temperature rise rate of concrete under adiabatic condition

4. Concrete temperature rise modeling

With the introduction of the reaction ratio of slag and the hysteresis temperature, an estimation method of adiabatic concrete temperature rise was proposed by Tanaka [9]. With the method, the exothermic characteristics of blastfurnace slag blended cement with arbitrary replacement ratio of blast furnace slag can be estimated. Considering the possible inherent difference of OPC and GGBS, a coefficient β was introduced for the equation of heat of hydration:

$$H = \beta H_o [1 - e^{(-\alpha t)}] \quad (1)$$

where H_o is final heat value, α is the coefficient relating to exothermic velocity, and t is time. Coefficient β was obtained when the equation (1) is used to fit the test results of the adiabatic temperature rise of the concrete in the study.

Figure 3 shows the typical adiabatic temperature curves from testing and prediction. The modified estimation method may be used to describe the exothermic characteristics of the concrete in the study. The generated heat value from Equation (1) will be used as the heat source in the next section to simulate heat transfer in concrete mass block.

5. Concrete temperature rise FDM simulation, results and discussion

In Cartesian coordinates, the heat equation is generally expressed as:

$$\frac{\partial}{\partial x} \left(k \frac{\partial T}{\partial x} \right) + \frac{\partial}{\partial y} \left(k \frac{\partial T}{\partial y} \right) + \frac{\partial}{\partial z} \left(k \frac{\partial T}{\partial z} \right) + \dot{q} = \rho c_p \frac{\partial T}{\partial t} \tag{2}$$

where \dot{q} is the rate at which energy is generated per unit volume of the medium; T is the temperature distribution T(x,y,z) as a function of time t; ρ is the density of the medium; c_p is the specific heat; and k is the thermal conductivity of the medium.

For the transient conduction numerical analysis, Equation (2) can be solved by the finite-difference method (FDM) [10]. In this paper, two-dimensional FDM analysis is used to simulate the heat conduction in concrete trial block. The middle square section plane is taken for consideration (Figure 4). This is obviously an approximate approach due to the implication of no heat loss assumption in the third direction. Due to the low value of the thermal conductivity of concrete material, if the size of the concrete trial block is big enough, it maybe appropriate to consider the middle section plane as a case of two-dimensional heat conduction.

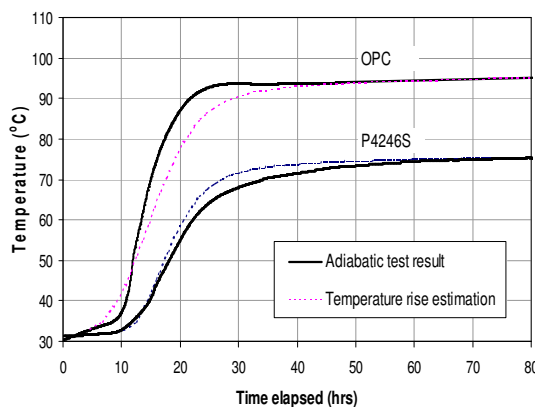


Figure 3. Prediction of adiabatic temperature rise of concrete (P4246S, cement content 405kg/m³)

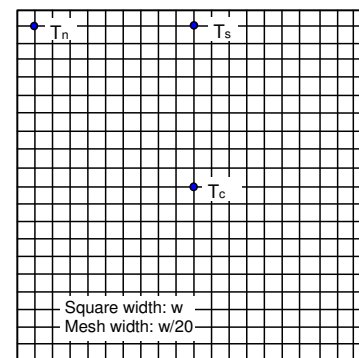


Figure 4: 2D FDM modeling for heat transfer analysis

To simulate the temperature rise in concrete block, HSPBFC cement with 70% GGBS was taken as the heat sources of the concrete. Concrete thermal conductivity is assumed as a constant value for the fresh concrete. Specific heat of the concrete was calculated from the mix proportion design. The concrete block is normally insulated and supported by the insulation material and formwork. Sometimes the steel formwork is used and yields poor insulation to the concrete mass. For simplicity of the analysis, the physical conditions existing at the boundaries was handled with air convection regardless of the particular nature of the convection heat transfer and the conduction heat transfer, even though the actual concrete block is never directly exposed to the ambient environment. Two extreme cases are analogous to the actual conditions. One is the case of fully insulated surface. This is equivalent to the air convection coefficient $h = 0$. And another case is the adoption of steel formwork. Due to the relatively very high thermal conductivity of steel, the generated heat can be lost very fast from the concrete surface. This is equivalent to the case of concrete surface fully exposed to ambient environment ($h = 20W/m^2 \cdot ^\circ C$). The convection coefficient $h = 0 \sim 20W/m^2 \cdot ^\circ C$ is adapted to study the effects of boundary conditions on the temperature distribution in concrete. This is equivalent to the air free convection conditions [10]. Other numerical analysis study [3] used $4.8W/m^2 \cdot ^\circ C$ and $23W/m^2 \cdot ^\circ C$ as the convection coefficients for the concrete with formwork and

exposure to air, respectively. The related thermal properties used in the analysis are tabulated in Table 4.

Table 4: Thermal properties of concrete used in the analysis

Properties	Values	Reference
Unit weight	2350 kg/m ³	-
Cement content	405 kg/m ³	-
w/c ratio	0.42	-
Thermal conductivity	2.0 W/m.K	[2]
Specific heat	960 J/kg.°C	-
Convection coefficient, h	0 ~ 20 W/m ² .°C	[3, 10]
Heat generation	Equation (1)	-
Placing temperature	32 °C	-
Ambient temperature	30 °C	-

5.1 Effects of size of concrete block and boundary conditions

The results of maximum core temperature T_c in concrete with different boundary conditions are shown in Figure 5. The maximum temperature at $h = 0$ is the temperature at 72hr under adiabatic conditions. The maximum temperature at center heavily depends on the insulation and the size of the trial block ($w =$ square width). The results indicate that the center of a 2 X 2 X 2m trial concrete block with proper insulation could produce the maximum core temperature T_c very close to that under adiabatic condition. This implies that the maximum temperature at the center of a concrete block is little affected by the size of the concrete if the dimension is big enough.

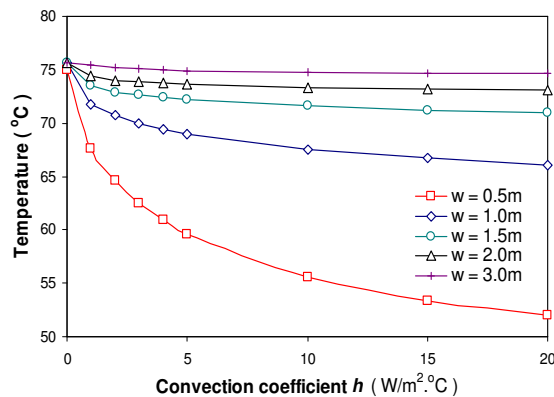


Figure 5: Maximum temperature at the center of concrete block

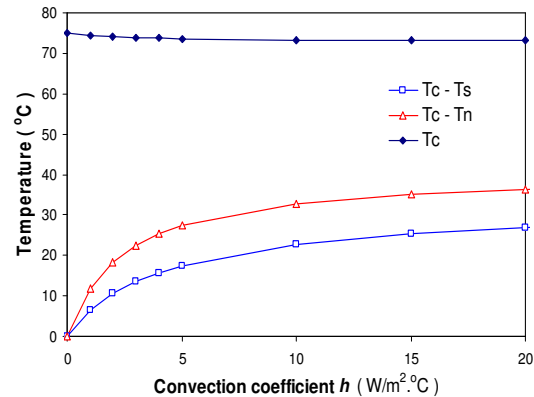


Figure 6: Maximum temperature difference (2 x 2 x 2m concrete block)

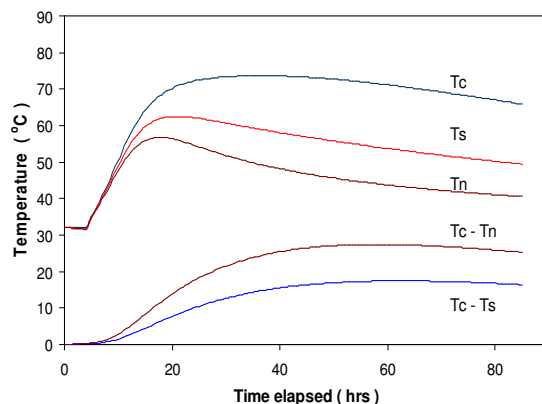


Figure 7: Typical temperature rise curves in concrete block ($h = 5.0$ W/m². °C)

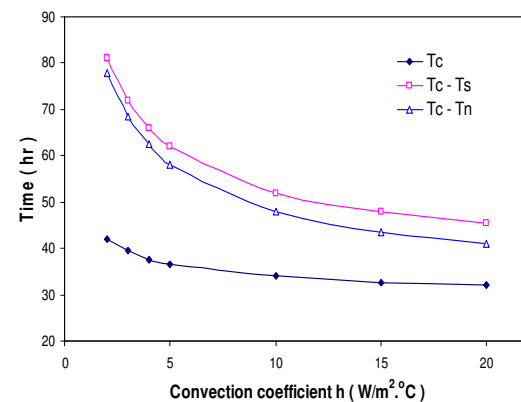


Figure 8: Effect of boundary conditions on the timing of peak temperature

Figure 6 presents the maximum temperature difference of $(T_c - T_n)$ and $(T_c - T_s)$ in a 2 x 2 x 2m concrete block. The results reveal that the degree of insulation plays a dominant role in controlling the maximum temperature difference across the block, even though the core temperature varies marginally. Direct exposure of concrete surface to air or the use of steel formwork is detrimental, because the maximum temperature differences $(T_c - T_n)$ and $(T_c - T_s)$ could easily exceed 20°C.

5.2 Temperature rise and temperature distribution

Typical temperature rise curves are shown in Figure 7. Due to the greater heat loss rate at corner and side of the block, the temperatures at corner and side reach the peak before the maximum core temperature. The center temperature begins to decrease when the heat generated in block is not enough to compensate the heat loss to the environment. After the decrease of the core temperature, the temperature difference $(T_c - T_n)$ and $(T_c - T_s)$ gradually climb to the peak. This is normally regarded as the critical period for the surface concrete. Situations would become even worse if the formwork is removed during this stage. Figure 8 demonstrates the effect of the boundary conditions on the time of peak temperature. The results show that the poor insulation could significantly reduce the time to reach the maximum temperature differences of $(T_c - T_n)$ and $(T_c - T_s)$. This infers that poorly insulated mass concrete could develop thermal cracks shortly after the placement.

The heat loss variation due to the temperature variation during daytime and nighttime was simulated by the boundary condition $h = 5 + 2\sin(\pi t/12)$. The temperature rise curves are presented in Figure 9, and the resulted values are tabulated in Table 5. The temperature at center is little affected by the environment variation due to the big enough size while the temperature difference $(T_c - T_n)$ and $(T_c - T_s)$ is affected in some degree. The maximum value of $(T_c - T_n)$ increases by 0.9°C while that of $(T_c - T_s)$ increases by 0.7 °C. The duration of the maximum $(T_c - T_n)$ and $(T_c - T_s)$ is also affected. This suggests that, during the course of insulation selection, it is necessary to consider the environment heat loss variation to minimize the effect.

Table 5: Analysis results of the temperature rise

Convection coefficient (W/m ² .°C)	Max. T _c (°C)	Max. (T _c - T _s) (°C)	Max. (T _c - T _n) (°C)
5	73.6	17.5	27.4
5 + 2 sin(π t/12)	73.7	18.2	28.3

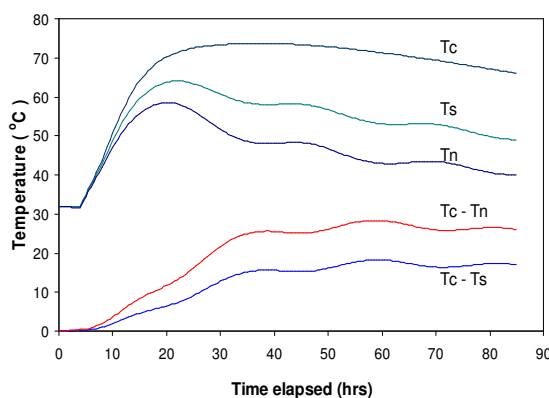


Figure 9: Temperature rise in concrete

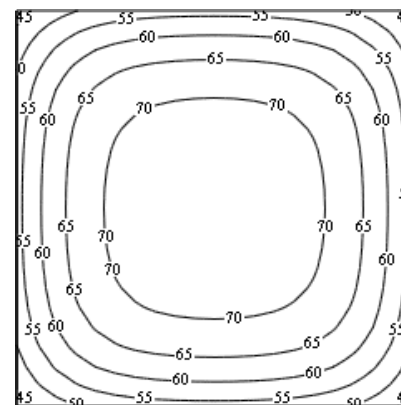


Figure 10: Temperature distribution contour (in °C) (h = 5.0 W/m².°C)

The typical temperature distribution contour at the time of peak core temperature is shown in Figure 10. Four corners are “cold” because of the heat loss in more than one direction, and this makes them the most dangerous places of thermal cracking. The situation would be even worse for actual mass concrete block and concrete structures due to the three-dimensional heat loss at corner.

It is thus inferred that temperature gradient of actual concrete structures could be improved by additional insulation at edges and corners. The temperature gradient along the regions close to the side is much steeper than that in the central region. This suggests that the locations of the thermocouples in the concrete mockup block should be carefully defined so that the comparable results can be obtained.

5.3 Comparison with a concrete mockup test

For the evaluation of the temperature rise in mass concrete trial block, a 2 X 2 X 2m concrete block was cast. HSPBFC containing 73% GGBS was used for the C45 concrete. The cement content and water/cement ratio was 415kg/m³ and 0.37, respectively. The schematic drawing of the block is described in Figure 11, with the locations of the thermocouples indicated. 50mm timber formwork and 50mm polyfoam were adopted as the insulation to the concrete mass around the four sides. The top of the concrete was only covered with the polyfoam. T_c is the core temperature at center of the block while T_s and T_n represent the temperature at side and corner location as indicated in the schematic drawing. The temperature rise results are shown in Figure 12.

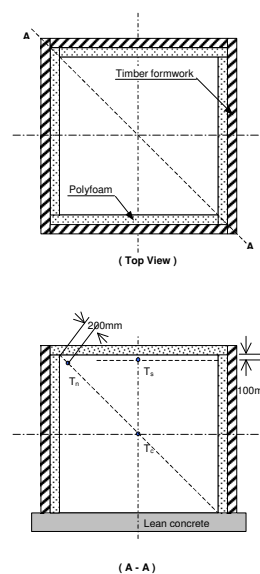


Figure 11: Mass concrete trial block

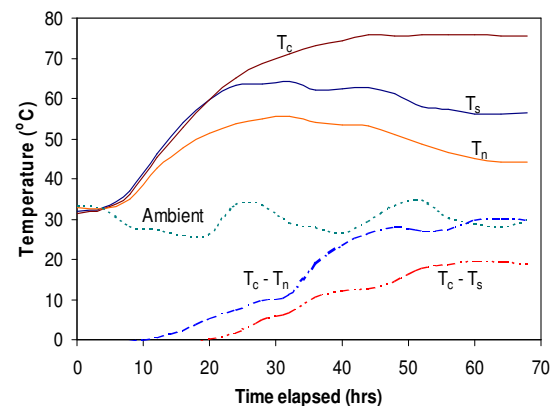


Figure 12: Temperature rise in concrete mockup

Figure 12 shows how the temperature gradient formed after the concrete mix placement. Temperature differential formed from the very beginning of the temperature rise in the concrete mass. Temperature at the corner of the block had the lowest value while the temperature at center gave the highest. $(T_c - T_n)$ is always greater than $(T_c - T_s)$. This may be explained as that the heat loss in the corner of the block is multi-dimensional. The peak value of $(T_c - T_n)$ and $(T_c - T_s)$ occurred after T_c . This implies that the maximum temperature difference was encountered in the cooling down period of the concrete mass. It is also clearly demonstrated in Figure 12 that the temperature differences of $(T_c - T_n)$ and $(T_c - T_s)$ were affected by the ambient temperature fluctuation, which is formed by the temperature change from daytime to nighttime. In this case, the maximum T_c is 76°C, and the maximum temperature differences of $(T_c - T_n)$ and $(T_c - T_s)$ are 30°C and 20°C, respectively.

6. Conclusion

1). Significant reduction of temperature rise and maximum temperature rise rate of HSPBFC concrete under adiabatic conditions was demonstrated in the experimental investigation. This indicates that the use of the HSPBFC concrete in mass concrete pours can be beneficial in minimizing the mass overheating and concrete cracking.

2). The modified estimation method can be used successfully to describe the characteristics of adiabatic temperature rise of the concrete in the study. If the concrete block is big enough ($\geq 2\text{m}$), the maximum core temperature would be very close to the peak adiabatic temperature.

3). The outcome of the numerical analysis suggests that good insulation is needed to minimize the temperature difference in mass concrete. In mass concrete pouring, additional insulation at edges and corners can help to improve temperature gradient in the critical regions. Moreover, hasty removal of the formwork during the concrete cooling down period may greatly increase the temperature gradient, and this could be detrimental to the surface of concrete mass.

Reference

- [1] Hunt J. G., *A laboratory study of early-age thermal cracking of concrete*, Technical report, Cement and Concrete Association, July 1971
- [2] Schutter G. D. and Taerwe L. (1996), Estimation of early-age thermal cracking tendency of massive concrete elements by means of equivalent thickness, *ACI Materials Journal*, Vol. 93, No. 5, pp 403-408.
- [3] Ayotte E., Massicotte B., Houde J., and Gocevski V., Modeling the thermal stress at early ages in a concrete monolith, *ACI Materials Journal*, 1997, Vol. 94, No. 6, pp 577-587.
- [4] Miao B., Chaallal O., Perraton D., and Aitcin P., On-site early-age monitoring high-performance concrete columns, *ACI Materials Journal*, 1993, Vol. 90, No. 5, pp 415-420.
- [5] Neville A. M., *Properties of concrete*, Longman, 4th ed., 1996
- [6] Corish A. T. and Cool M. J., Heat generation in blended cement concretes, 2nd *International Symposium on blended cements*, 1994, 10-11 Nov., Malaysia.
- [7] DD ENV 206:1992, *Concrete: performance, production, placing and compliance criteria*, BSI Standards
- [8] Yang J. L., Chen E. Y., Low G. L. and Tan B. T., Compressive strength of Portland blast furnace slag cement concrete in adiabatic and semi-temperature matched curing conditions, *Proceedings: Sixth International Conference CANMET / ACI / JCI*, 1998, SP-178-44, pp 857-873.
- [9] Tanaka S., Inoue K. Shimoyama Y., and Tomita R., Methods of estimating heat of hydration and temperature rise in blast furnace slag blended cement, *ACI Materials Journal*, 1995, Vol. 92, No. 4, pp 429-436.
- [10] Incropera F. P., *Introduction to heat transfer*, John Wiley & Sons, INC, 3rd ed., 1996